PLOS ONE

RESEARCH ARTICLE

^{18} F-FDG PET/MR imaging in patients with suspected liver lesions: Value of liver-specific contrast agent Gadobenate dimeglumine

Julian Kirchner[1]*, Lino M. Sawicki[1], Cornelius Deuschl[2], Johannes Grüneisen[2], Karsten Beiderwellen[2], Thomas C. Lauenstein[2], Ken Herrmann[3], Michael Forsting[2], Philipp Heusch[1], Lale Umutlu[2]

1 Department of Diagnostic and Interventional Radiology, University Dusseldorf, Medical Faculty, Dusseldorf, Germany, **2** Institute of Diagnostic and Interventional Radiology and Neuroradiology, University Hospital Duisburg-Essen, Germany, **3** Department of Nuclear Medicine, University Hospital Essen, University of Duisburg-Essen, Essen, Germany

* Julian.Kirchner@med.uni-duesseldorf.de

OPEN ACCESS

Citation: Kirchner J, Sawicki LM, Deuschl C, Grüneisen J, Beiderwellen K, Lauenstein TC, et al. (2017) ^{18} F-FDG PET/MR imaging in patients with suspected liver lesions: Value of liver-specific contrast agent Gadobenate dimeglumine. PLoS ONE 12(7): e0180349. https://doi.org/10.1371/journal.pone.0180349

Editor: Andreas-Claudius Hoffmann, West German Cancer Center, GERMANY

Received: February 15, 2017

Accepted: June 14, 2017

Published: July 6, 2017

Data Availability Statement: All relevant data are within the paper.

Funding: This research was supported in part by a sponsored research agreement with Bracco, Milano, Italy. The funder had no role in study design, data collection and analysis, decision to publish, or preparation of the manuscript

Competing interests: This research was supported in part by a sponsored research agreement with Bracco, Milano, Italy. This does not alter our

Abstract

Objectives

To evaluate the added value of the application of the liver-specific contrast phase of Gadobenate dimeglumine (Gd-BOPTA) for detection and characterization of liver lesions in ^{18}F-FDG PET/MRI.

Methods

41 patients with histologically confirmed solid tumors and known / suspected liver metastases or not classifiable lesions in ^{18}F-FDG PET/CT were included in this study. All patients underwent a subsequent Gd-BOPTA enhanced ^{18}F-FDG PET/MRI examination. MRI without liver-specific contrast phase (MRI_1), MRI with liver-specific contrast phase (MRI_2), ^{18}F-FDG PET/MRI without liver-specific contrast phase (PET/MRI_1) and with liver-specific contrast phase (PET/MRI_2) were separately evaluated for suspect lesions regarding lesion dignity, characterization, conspicuity and confidence.

Results

PET/MRI datasets enabled correct identification of 18/18 patients with malignant lesions; MRI datasets correctly identified 17/18 patients. On a lesion-based analysis PET/MRI_2 provided highest accuracy for differentiation of lesions into malignant and benign lesions of 98% and 100%. Respective values were 95% and 100% for PET/MRI_1, 93% and 96% for MRI_2 and 91% and 93% for MRI_1. Statistically significant higher diagnostic confidence was found for PET/MRI_2 and MRI_2 datasets compared to PET/MRI_1 and MRI_1, respectively ($p < 0.001$).

Conclusion

The application of the liver-specific contrast phase in ^{18}F-FDG PET/MRI further increases the diagnostic accuracy and diagnostic confidence for correct assessment of benign and malignant liver lesions.

adherence to PLOS ONE policies on sharing data and materials. The authors have declared that no competing interests exist.

Introduction

As the second most frequent organ manifestation of distant metastases [1], liver metastases are considered among the most common malignant liver lesions and occur approximately up to 18–40 times more frequent than primary liver malignancies [2]. Malignancies accounting for liver metastases are primarily lung cancer, breast cancer, colorectal cancer, and pancreatic carcinoma [3]. While the incidence of liver metastases significantly outnumbers the occurrence of hepatocellular carcinoma (HCC), HCC accounts for up to 80% of primary liver cancers [4] and is regarded as the sixth most common cancer worldwide and the third most common cause of cancer-related death [5]. Correct determination of the hepatic tumor-spread is crucial for optimized therapy stratification as potentially curative options are commonly restricted to resection. Furthermore, apart from malignant liver pathologies, benign lesions also demand correct identification as some liver lesions e.g. adenomas are known to be associated with potential complications such as hemorrhage, rupture or malignization [6–8]. Hence, high-quality liver imaging is crucial for best patient care and therapy management. While computed tomography (CT) and transabdominal ultrasound still represent the primary and most commonly applied imaging modalities, more advanced imaging techniques such as magnetic resonance imaging (MRI) have been shown superior for correct depiction and characterization of liver lesions when compared to ultrasound, CT and positron emission tomography / CT using ^{18}F-fluoredeoxyglucose [9–11]. Particularly the utilization of liver-specific contrast agents has been shown to provide important additional diagnostic information for assessment of small lesions $<$ 15mm, hepatocellular carcinoma as well as for correct discrimination of liver adenomas from focal nodular hyperplasias (FNH) [12–15]. Hence, in accordance with the ESGAR consensus statement on liver MR imaging the application of liver-specific contrast agents is recommended in patients considered for liver resection [16]. Apart from its excellent diagnostic capacity, MR imaging is restricted to morphological and functional information of lesions, lacking the metabolic component of PET imaging. With the successful introduction of integrated PET/MRI systems into clinical imaging [17], numerous studies have demonstrated the high diagnostic quality and potential superiority of PET/MRI in dedicated applications [18–21]. Reporting initial results, Beiderwellen et al demonstrated higher lesion conspicuity and diagnostic confidence in liver lesions in PET/MRI compared to PET/CT in a whole body staging approach [22]. Recent publications also investigated the added value of the utilization of liver-specific contrast agents in PET/MRI for detection of malignant liver lesions [23]. Thus, following these first results, the purpose of this study was to evaluate the added value of the liver-specific contrast phase of Gadobenate dimeglumine (MultiHance, Bracco, Milano, Italy) enhanced ^{18}F-FDG PET/MRI for detection and characterization of malignant and benign liver lesions.

Material & methods

Patients

The study was conducted in conformance with the Declaration of Helsinki and approved by the Ethics Commission of the Medical Faculty of the University Duisburg-Essen (study number 11-4822-BO). All patients underwent a clinically indicated whole-body ^{18}F-FDG-PET/CT (PET/CT) and subsequently an additional ^{18}F-FDG PET/MRI (PET/MRI) of the liver with application of Gadobenate dimeglumine (Gd-BOPTA) after informed written consent was obtained.

41 patients (mean age 55.9 ± 14.5 years; range 27–79) met the inclusion criteria of histologically confirmed solid tumors and known or suspected liver metastases or non-classifiable

Table 1. Demographic characteristics.

sex	number	mean age (years)
female	21	56.4 ± 16
male	20	54.3 ± 12.8

https://doi.org/10.1371/journal.pone.0180349.t001

lesions in PET/CT (Table 1). Exclusion criteria were patient age <18 years and contraindication to MRI such as pacemaker or chronic renal failure. Primary tumors included primary liver tumors as well as extrahepatic tumors (Table 2).

PET/MRI

^{18}F-FDG PET/MRI examinations were performed on an integrated 3 Tesla PET/MRI scanner (Biograph mMR, Siemens Healthcare GmbH, Erlangen, Germany) subsequently after clinically indicated ^{18}F-FDG PET/CT examinations and obtained with an average delay of 153 ± 35 min (range: 96 min—138 min) after intravenous injection of body-weight adapted mean activity of 244 MBq ± 53 MBq (range: 106 Mbq—382 Mbq) ^{18}F-FDG. No additional tracer was injected for the subsequent ^{18}F-FDG PET/MRI examinations. The liver-specific contrast phase was acquired on average 74 ± 25 (range 58–122 min) after contrast media application. Scan volumes covered the whole liver.

PET data acquisition was performed for early phase datasets as well as for liver-specific contrast phase datasets in 1 bed position with 10 minutes. PET images were reconstructed using the iterative ordered-subset expectation maximization (OSEM) algorithm, 3 iterations and 21 subsets, a Gaussian filter with 4mm full width at half maximum (FWHM) and a 344 × 344 image matrix. For MR-based signal intensity correction a two-point (fat, water) coronal 3D-Dixon-VIBE (volumetric interpolated breath-hold examination) sequence was performed to generate a four-compartment model (background air, lungs, fat, muscle) [24]. The pre-contrast MRI sequences were obtained simultaneously using a 24-channel spine-array radiofrequency coil as well as 16-channel flex body-coils, depending on patient size. After completion of PET-acquisition, additional Gd-BOPTA enhanced sequences were acquired. The following imaging protocol was applied (Fig 1):

1. A coronal T1-w 3D-Dixon-VIBE sequence prior contrast administration for attenuation correction only.
2. Am axial T1-w FLASH (fast low-angle shot) in- and opposed phase in breath-hold technique with a slice thickness of 7 mm (Echo Time [TE] 2 & 3.4 ms; Repetition Time [TR] 111 ms; Field of View [FOV] 400 mm; phase FOV 75%; acquisition matrix 256 × 192; in plane resolution 0.8 × 0.8 mm)

Table 2. List of primary tumors.

	n	%
Colorectal Carcinoma	19	46
Hepatocelluar Carcinoma	4	10
Melanoma	4	10
Cholangiocellular Carcinoma	3	7
Breast Cancer	2	5
Other	9	22
Total	41	100

https://doi.org/10.1371/journal.pone.0180349.t002

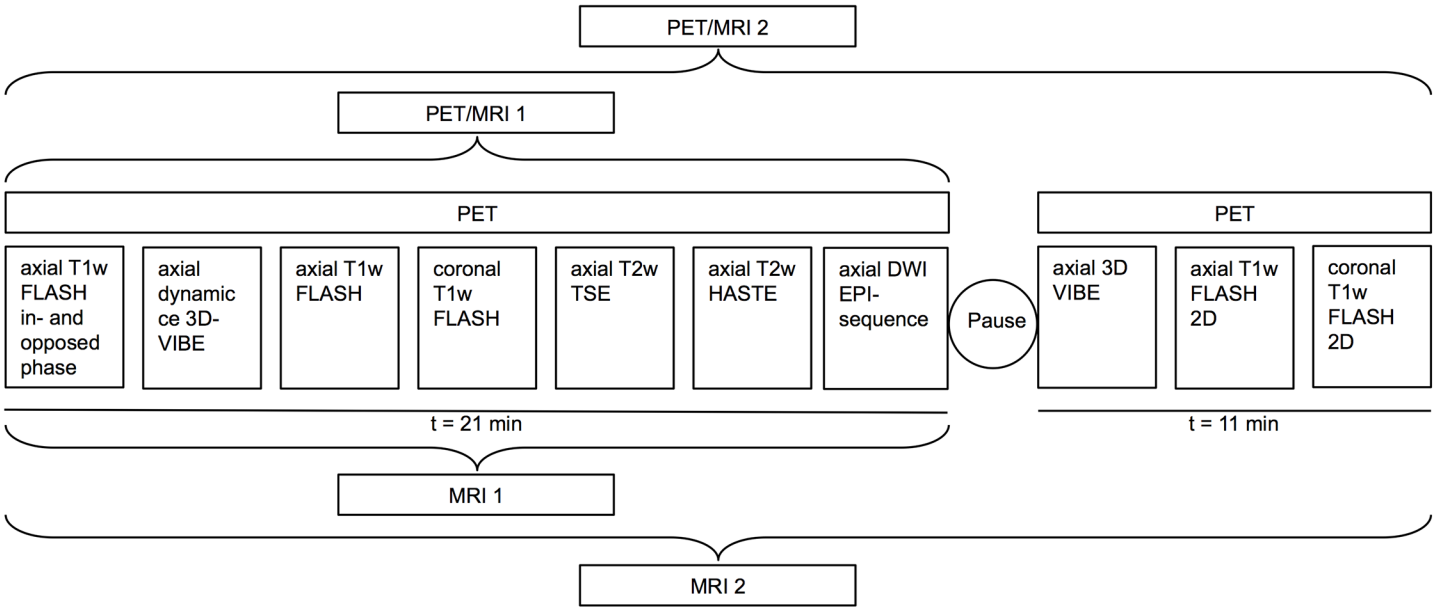

Fig 1. Overview of the imaging protocol and timing of each image acquisition. T1w VIBE = T1-weighted Volume-Interpolated Breath-hold Examination; T2w HASTE = T2-weighted Half Fourier Acquisition Single Shot Turbo Spin Echo; T1w FLASH = T1-weighted Fast Low-angle Shot; T2w TSE = T2-weighted Turbo-spin Echo; DW EPI = Diffusion-weighted Echo-Planar imaging.

https://doi.org/10.1371/journal.pone.0180349.g001

3. An axial dynamic contrast-enhanced 3-dimensional Volumetric Interpolated Breath-hold Examination (VIBE) with a slice thickness of 3.5 mm (TE, 1.5 ms; TR, 4 ms; Flip angle 9°; FOV 400 mm; phase FOV 75%; acquisition matrix 512 × 384, in plane resolution 0.8 x 0.8 mm) before and 20s, 50s and 80s after intravenous administration of Multihance (0,05 mmol/kg bw)
4. An axial T1-w FLASH 2D fat-saturated in breath-hold technique with a slice thickness of 7mm (TE, 3.62 ms; TR 185 ms; FOV 400 mm; phase FOV 75%; acquisition matrix 320 × 240, in plane resolution 1.3 x 1.3 mm)
5. A coronal T1-w FLASH 2D fat-saturated in breath-hold technique with a slice thickness of 6 mm (TE, 2.49 ms; TR 125 ms; FOV 360 mm; phase FOV 100%; acquisition matrix 256 × 256, in plane resolution 1.4 x 1.4 mm)
6. An axial T2-w TSE (Turbo-spin Echo) fat-saturated in breath-hold technique with a slice thickness of 7 mm (TE 97 ms; TR 2840 ms; FOV 400 mm; phase FOV 750%; acquisition matrix 256 × 192, in plane resolution 1.6 x 1.6 mm)
7. An axial T2-w HASTE (half Fourier acquisition single shot turbo spin echo) in breath-hold technique with a slice thickness of 7 mm (TE 100 ms; TR 1000 ms; Turbo factor (TF) 194; FOV 400 mm; phase FOV 75%; acquisition matrix 320 × 240 mm; in plane resolution 1.3 x 1.3 mm)
8. An axial diffusion-weighted echo-planar imaging (EPI) sequence in free breathing with a slice thickness of 5.0 mm (TR 8000 ms; TE 81 ms; b-values: 0, 500 and 1000 s/mm2, matrix size 192 x 156; FOV 420 mm, phase FOV, 81.3%; GRAPPA, acceleration factor 2; in plane resolution 2.2 x 2.2 mm)

Pause and subsequently acquired liver-specific phase.

9. A coronal T1-w 3D-Dixon-VIBE sequence for attenuation correction only.
10. An axial 3D VIBE with a slice thickness of 3.5 mm (TE 1.5 ms; TR 4 ms; Flip angle 9°; FOV 400 mm; phase FOV 75%; acquisition matrix 512 × 384, in plane resolution 0.8 x 0.8 mm).
11. An axial T1w FLASH 2D fat-saturated in breath-hold technique with a slice thickness of 7 mm (TE 3.62 ms; TR 185 ms; FOV 400 mm; phase FOV 75%; acquisition matrix 320 × 240, in plane resolution 1.3 x 1.3 mm)
12. A coronal T1w FLASH 2D fat-saturated in breath-hold technique with a slice thickness of 6 mm (TE 2.49 ms; TR 125 ms; FOV 360 mm; phase FOV 100%; acquisition matrix 256 × 256, in plane resolution 1.4 x 1.4 mm)

Image analysis

The following imaging datasets of the ^{18}F-FDG PET/MR examination were analysed in consensus and in random order by two experienced radiologists in hybrid and MR imaging interpretation on a dedicated OsiriX Workstation (Pixmeo SARL, Bernex, Switzerland): MRI without liver-specific contrast phase (MRI_1), MRI with liver-specific contrast phase (MRI_2), ^{18}F-FDG PET/MRI without liver-specific contrast phase (PET/MRI_1) and with liver-specific contrast phase (PET/MRI_2). All datasets were evaluated in two reading sessions in random order and both readers were blinded to patient identity and results of prior or follow-up imaging. In a first reading session radiologists evaluated MRI_1 and subsequently MRI_2. In a second reading session with a minimum of four weeks apart to avoid recognition bias, PET/MRI_1 and subsequently PET/MRI_2 were evaluated. Interpretation was performed patient- and lesion-based. In conformity to previous studies [22] every liver lesion in each patient was rated with regard to lesion dignity (1, benign; 2, malignant), lesion conspicuity (5-point ordinal scale: 1, not visible; 2, very low contrast; 3, low contrast; 4, intermediate contrast; 5, high contrast) and diagnostic confidence (5-point ordinal scale: 1, very low confidence; 2, low confidence; 3, indeterminate confidence; 4, high confidence; 5, very high confidence).

Gadobenate dimeglumine differs from extracellular gadolinium agents as a fraction of 3–5% of the injected dose is taken up into functioning hepatocytes, entailing long-lasting enhancement of the normal liver parenchyma that results in significantly increased sensitivity and characterization for liver lesions in T1-weighted images between 40 and 120 minutes after intravenous administration [25,26]. Hence, Gadobenate dimeglumine and other so-called liver-specific contrast agents have been demonstrated to enable an improved detection and differentiation of small metastases and HCCs as well as an improved differentiation of benign liver lesions, such as liver adenomas from FNH [27]. According to the ESGAR consensus statement on liver, MRI liver-specific contrast agents are recommended to be applied in pre-surgical work up of hepatic lesions for lesion detection and characterization, particularly when the differential diagnosis is primarily between solid benign lesion (e.g. FNH) versus metastasis and for clear delineation of primary liver tumors [16]. As metastatic involvement of the liver is known to lead to major changes in therapy management, correct identification of the extent of hepatic tumor spread is of utmost importance in a pre-therapeutic setting as well as in a post-surgical setting since incomplete resection does not prolong survival [28] (Fig 1E–1H). Furthermore, in contrary to most benign liver lesions, that do not require resection or follow-up, liver adenomas demand correct characterization, as they are known to bear the risk of spontaneous rupture or degeneration to hepatocellular carcinoma [29].

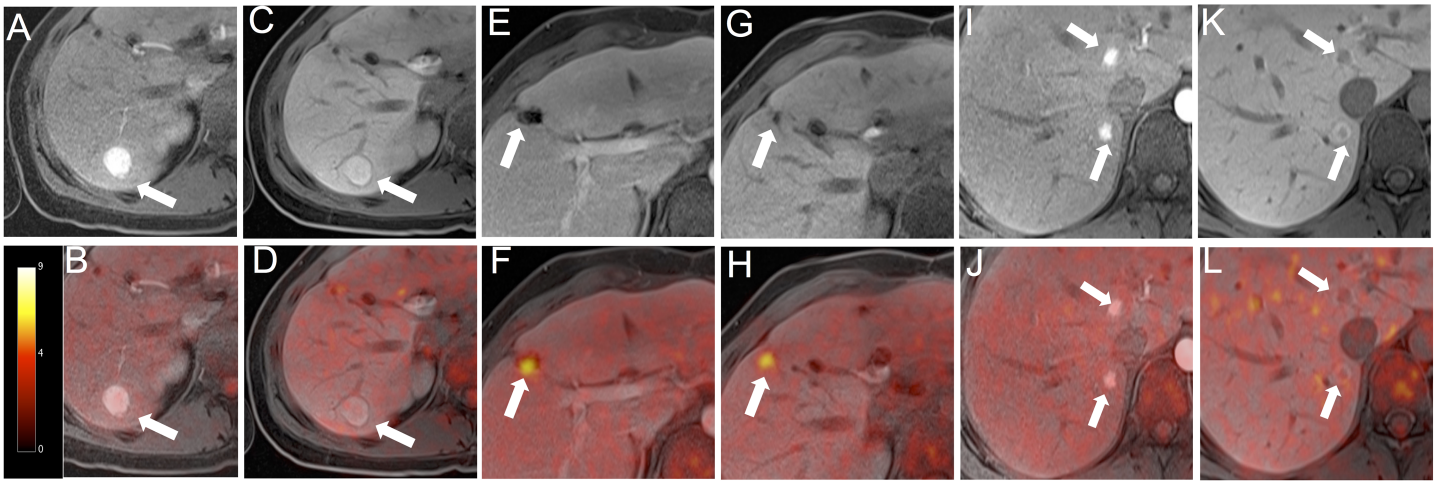

Fig 2. A 25-year-old female patient with a history of colorectal cancer presented multiple liver lesions after surgery. The FNH in the right liver shows an arterial contrast-agent enhancement (A) and is still hyperintense in the liver-specific contrast phase (C). No significant ^{18}F-FDG-uptake is seen (B, D). A second lesion in the right liver is rated as a colorectal liver metastasis due to incomplete resection. Tumor lesion is neither detectable by MRI without liver-specific contrast phase nor with liver-specific contrast phase (E; G). In fused PET/MR images (F; H) the remaining tumor tissue lesion could clearly be identified. Additional lesions near the liver hilus are adenomas with strong arterial contrast-agent enhancement (I). In the liver-specific contrast phase lesions are hypointense (K). Similar to the FNH, no significant ^{18}F-FDG-uptake is seen (J, L).

https://doi.org/10.1371/journal.pone.0180349.g002

For the characterization of the focal liver lesions detected in each interpreting session, the readers were asked first to decide whether a lesion was benign or malignant and to then give a diagnosis, in terms of characterization of the lesions. Malignant lesions comprised hepatocellular carcinoma (HCC), cholangiocellular carcinoma (CCC) and metastasis. Benign lesions comprised cyst, haemangioma, focal nodular hyperplasia, adenoma and regenerating nodule (Fig 2). The readers were given information about the primary tumor localization, as liver metastases originating from different tumors may show different contrast enhancement patterns. Lesion characterization was performed based on all available T1 and T2 weighted sequences as well as DWI. A potential diffusion restriction with corresponding signal drop in the ADC map was considered indicative for malignancy.

For lesion characterization on PET, visually increased focal ^{18}F-FDG-uptake in comparison to surrounding tissue was considered indicative of malignancy (PET-positive lesions). In accordance with previous publications lesions were rated as metastases when at least two of the three following criteria in MRI_1 and PET/MRI_1 or rather three of the four following criteria in in MRI_2 and PET/MRI_2 were found: (1) Hyperintense lesion in T2w images with ill-defined borders, (2) diffusion restriction on DWI, (3) contrast behaviour not inkeeping with cysts, hemangioma, FNH or adenoma and (4) hypointense lesion in liver-specific phase [30,31].

In all lesions demonstrating focal ^{18}F-FDG uptake the maximum standardized uptake value (SUVmax) was measured by placing a manually drawn polygonal volume of interest (VOI) over each lesion on attenuation-corrected PET images. Additionally, the maximum discernible diameters of all suspicious lesions were determined in the liver-specific contrast phase. In accordance with previous publications reporting the superiority of PET uptake over morphology [32] as well as the high sensitivity for detection of malignant lesions in MRI when utilizing the liver-specific contrast phase [33], discrepant findings on PET and MR datasets as well as discrepancies between the two readers, a consensus decision among the two readers was made based on all available data.

Reference standard

Histopathological confirmation of the primary tumors was available in all patients except for the ones suffering from cancer unknown primary (CUP). In accordance with current treatment guidelines and ethical considerations, histopathological correlation for each depicted suspicious liver lesion was not clinically indicated and hence not available. A consensus characterization for each lesion based on available prior examinations, histopathological data, PET/CT, PET/MRI as well as imaging and clinical follow-up served as the standard of reference (mean interval of 295 ± 343 days).

Statistical analysis

Statistical analysis was performed using IBM SPSS version 22 (IBM Inc, Armonk, NY, USA).

Data analysis was performed patient-based as well as lesion based. The scores of resulting datasets were analysed first on a descriptive basis. Due to the ordinal scale scores the median scores were subsequently compared with the Friedman test. As post hoc test Wilcoxon signed-rank test was chosen and Bonferroni adjustment was applied.

Results

Patient based analysis

Based on the reference standard liver lesions were present in 36 / 41 patients (88%). Malignant liver lesions were present in 18 patients (44%), benign lesions in 27 patients (66%). Based on MRI alone (MRI_1 and MRI_2) 17 patients (94%) with malignant lesions could be correctly identified with one false-positive rating (4%). Both PET/MRI datasets (PET/MRI_1 and PET/MRI_2) enabled a correct identification of all 18 patients (100%) with malignant liver lesions.

Lesion-based analysis

Based on the reference standard a total of 137 lesions were detected. These comprised 80 (58%) benign and 57 (42%) malignant lesions (Table 3). All lesions could be detected in the readings including the liver-specific contrast phase (MRI_2 and PET/MRI_2), while one lesion was missed in the readings without the liver-specific contrast phase (MRI_1 and PET/MRI_1). The missed lesion in the datasets without the liver-specific contrast phase was due to a 6 mm, subcapsular lesion without FDG-uptake, that was only clearly discernible based on its hypointense appearance in the liver-specific phase (Fig 3). Highest accuracy for differentiation between malignant and benign lesions was achieved based on the PET/MRI_2 datasets, entailing a correct classification of 98% of the malignant and 100% of the benign lesions. The respective

Table 3. Lesion character in benign liver lesions in accordance to reference standard.

	n	%
Liver cyst	42	52.5
Hemangioma	11	13.75
Focal nodular hyperplasia	9	11.25
Scar tissue	6	7.5
Avital metastases	5	6.25
Adenoma	4	5
Regenerative nodule	2	2.5
Inflammatory	1	1.25
Total	80	100

https://doi.org/10.1371/journal.pone.0180349.t003

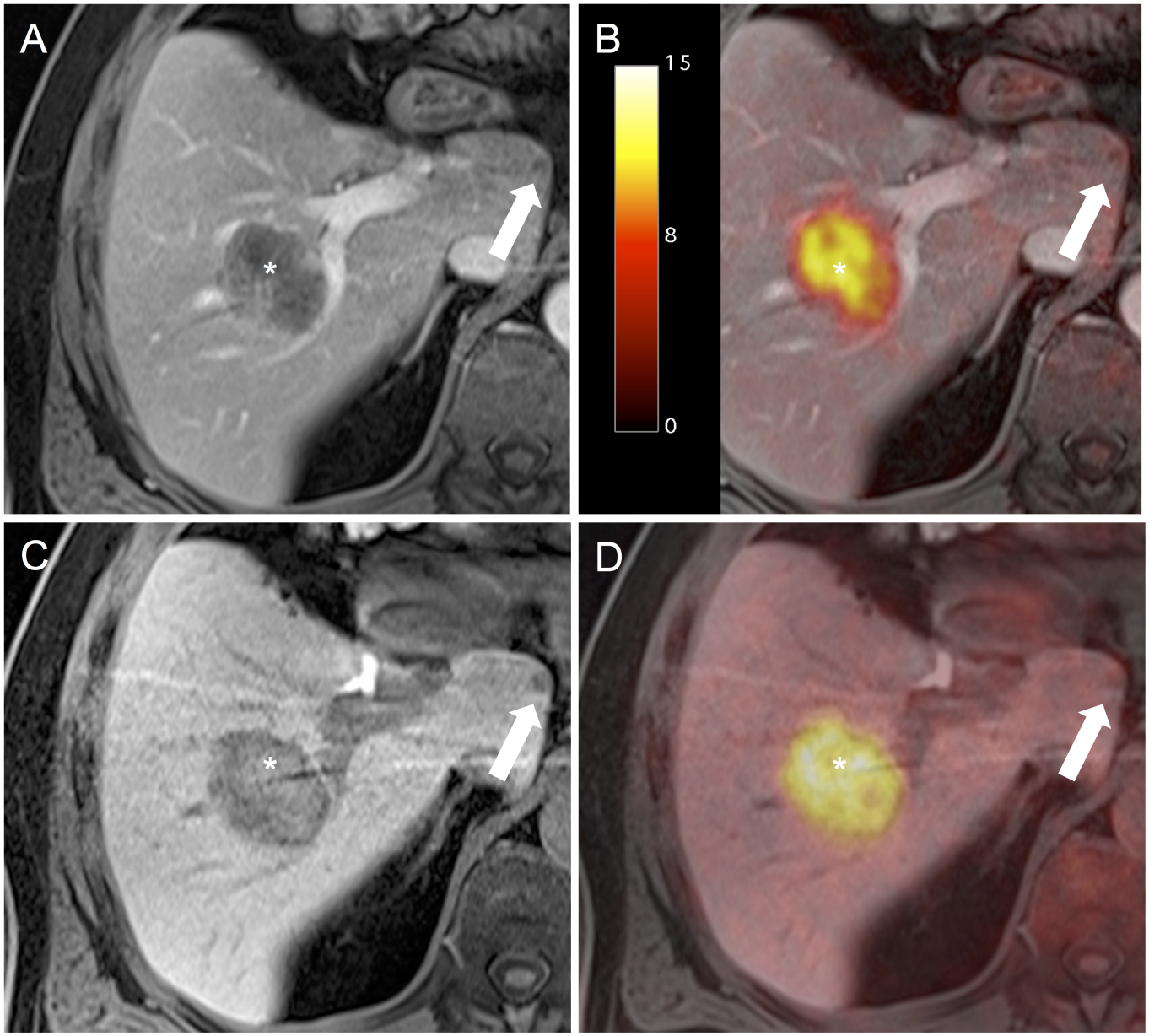

Fig 3. A 61-year-old male patient with liver metastases from a Colorectal Carcinoma. The large metastasis with intense ^{18}F-FDG-uptake in the right central liver lobe is clearly visible in all datasets (*). The metastasis in the Lobus caudatus does not show increased ^{18}F-FDG-uptake (A, D) and is hardly detectable in the arterial-phase (B) but is clearly detectable as hypointense lesion in the liver-specific phase (C).

https://doi.org/10.1371/journal.pone.0180349.g003

values for PET/MRI$_1$ were 95% and 100%, for MRI$_2$ 93% and 96% and 91% and 93% for MRI$_1$ (Table 4). The missed lesion in PET/MRI$_2$ was due to a 7 mm lesion without significant tracer uptake or clear diffusion restriction, which was falsely rated as a hemangioma and emerged as a metastasis in follow-up imaging.

Based on both readings including the liver specific phase (PET/MRI$_2$ and MRI$_2$) correct classification of all (100%) benign lesions was possible, while the exclusion of the liver-specific contrast phase (PET/MRI$_1$ and MRI$_1$) enabled a correct classification of 96% of the benign

Table 4. PET/MRI with liver specific-contrast phase (PET/MRI_2) offers highest accuracy for lesion classification in malignant and benign compared to PET/MRI without liver-specific phase (PET/MRI_1) and MRI with (MRI_1) and without liver-specific phase (MRI_2).

Lesions	MRI_1 (%)	MRI_2 (%)	PET/MRI_1 (%)	PET/MRI_2 (%)
Malignant *n* = 57	52 (91)	53 (93)	54 (95)	56 (98)
Benign *n* = 80	77 (96)	77 (96)	80 (100)	80 (100)
Total *n* = 137	129 (94)	130 (95)	134 (98)	136 (99)

Total numbers and the percentage (in parentheses) of correct classification in malignant and benign lesion for every modality are given.

https://doi.org/10.1371/journal.pone.0180349.t004

lesions (Table 5). Misclassifications in datasets without liver-specific phase were due to mischaracterization of FNH and adenoma.

Diagnostic confidence & lesion conspicuity

There was a statistically significant difference in the resulting scores for diagnostic confidence ($p < 0.001$) (Fig 4). Post hoc analysis with Wilcoxon signed-rank test was conducted with a Bonferroni correction applied, resulting in a significance level set at $p < 0.0125$. The score for MRI_2 was significantly higher compared to MRI_1 (MRI_2: median 5, range 2–5; MRI_1: median 4; range 1–5; $p < 0.001$) as well as to PET/MRI_1 (PET/MRI_1: median 4; range 1–5; $p < 0.001$). The score for PET/MRI_2 was significantly higher compared to MRI_1 (PET/MRI_2: median 5, range 2–5; $p < 0.001$) and PET/MRI_1 ($p < 0.001$). No statistically significant difference was shown between MRI_2 and PET/MRI_2 regarding the diagnostic confidence ($p = 0.18$). No statistically significant difference was detected between the modalities regarding lesion conspicuity ($p = 0.88$).

Discussion

Our results demonstrate the feasibility and high diagnostic performance of Gd-BOPTA enhanced ^{18}F-FDG PET/MRI and the additional value of the liver-specific contrast phase for depiction and characterization of liver lesions. This publication comprises two main messages we believe to be important: First, the accuracy in differentiating benign from malignant liver lesions in Gd-BOPTA enhanced ^{18}F-FDG PET/MRI with an additional liver-specific contrast phase is superior to the accuracy in Gd-BOPTA enhanced ^{18}F-FDG PET/MRI without an additional liver-specific contrast phase as well as in Gd-BOPTA enhanced MRI alone with and / or without an additional liver-specific contrast phase. Secondly, the application of a liver-specific contrast phase enables improved differentiation between potentially therapy-requesting liver adenomas and other benign liver lesions.

Hybrid imaging, in terms of PET/MRI, combines the high spatial resolution and soft-tissue contrast of MRI with the metabolic information based on the PET dataset. Recent studies demonstrated the high lesion conspicuity and diagnostic confidence in PET/MRI regarding liver lesions in a whole body approach [22] and its significantly higher diagnostic accuracy in the detection of liver metastases when compared to PET/CT [31].

Table 5. Correct classification of benign lesion in the different modalities in percentage.

	MRI_1	MRI_2	PET/MRI_1	PET/MRI_2
in %	96	100	96	100

https://doi.org/10.1371/journal.pone.0180349.t005

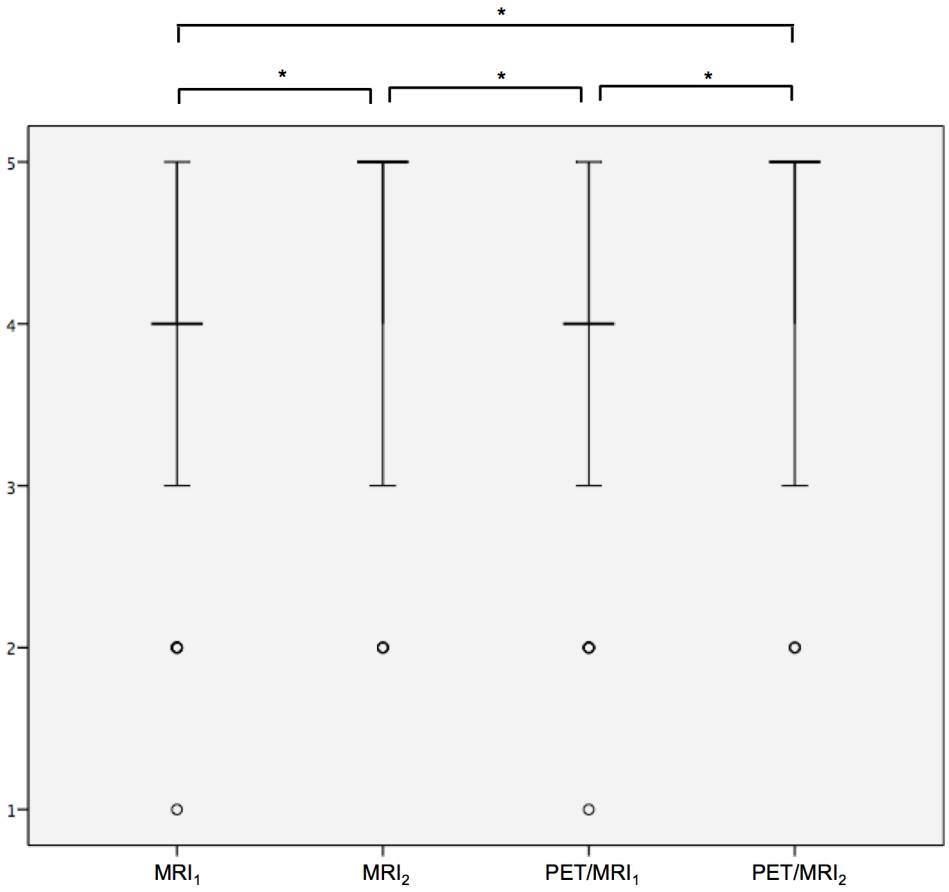

Fig 4. Diagnostic confidence is significantly higher in PET/MRI$_2$ and MRI$_2$ datasets compared to PET/MRI$_1$ and MRI. Ratings for lesion conspicuity are entered on the y-axis. The vertical bar represents the upper and lower quartiles; the horizontal bar represents the median. The points represent extreme values. Significant differences are marked by a star.

https://doi.org/10.1371/journal.pone.0180349.g004

Initial trials on detection and characterization of liver lesions have focused on the general comparison of PET/MRI and PET/CT [22,31] or MRI and PET/CT [9] as well as the added value of diffusion weighted imaging in liver MRI [34–36] without putting the focus on the value of liver-specific contrast agents. Recent trials have investigated the added value of liver-specific contrast agents for the differentiation of benign and malignant liver lesion in hybrid PET/MR imaging [23,37]. Donati et al reported their results on retrospective PET-MRI fusion in patients undergoing PET/CT and subsequent liver MRI with a liver specific contrast agent (Gd-EOB-DTPA) [37]. Comparable to our results, the authors reported a higher accuracy in detection and correct determination of the lesions dignity in (retrospectively fused) PET/MRI over MRI alone (93% vs. 91%). But Donati et al only divided the lesions in malignant and benign and forego to give the exact diagnosis. Furthermore they omitted the application of diffusion-weighted imaging. A study including this highly-appreciated imaging technique was published by Lee et al [23]. In this study the authors evaluated the diagnostic performance of integrated ^{18}F-FDG PET/MRI in the detection of colorectal cancer liver metastases.

Diffusion-weighted imaging has been well-established for liver imaging in the past years, and while it has become a valuable imaging method particularly for the detection of liver metastases, it is still recommended to be used as an adjunct to contrast-enhanced liver MRI in lieu of a stand-alone tool due to significant overlaps between ADC values of benign and

malignant lesions [16]. Hence, current guidelines recommend the combined application of DWI and liver-specific enhanced MRI for detection of (small) metastases [16]. Comparable to our results, Lee et al demonstrated the superiority of ^{18}F-FDG PET/MRI over MRI (each enhanced with liver-specific contrast agent) for detection of liver metastases, yet failing to merit significant difference. Our study differs in two points from Lee et al. First, in contrary to Lee et al, who only included patients suffering from colorectal carcinoma resulting in a mostly homogenous appearance of suspected malignancies, the patients in our study suffered from a wide range of primary malignancies, resulting in a potentially more diverse and hence more difficult to characterize, delineation of metastases. Secondly, we additionally investigated the diagnostic value of the liver-specific contrast phase not only for detection and differentiation of malignant from benign lesions but also for dedicated characterization of benign lesions. According to our results, the utilization of the liver specific phase enabled the highest diagnostic accuracy for detection and differentiation of malignant from benign lesions in ^{18}F-FDG PET/MRI and superior diagnostic accuracy when comparing MRI alone (with liver-specific contrast phase versus without liver-specific contrast phase). Furthermore, the utilization of the liver specific phase also led to an improved differentiation of liver adenomas from FNH, a differentiation with important clinical and therapeutic impact. This goes in line with previous publications underlining the diagnostic benefit of liver specific contrast agents for characterization of benign liver lesions and improvement of the diagnostic confidence. Gazioli et al reported specificity rates for differentiation of FNH, adenoma and liver adenomatosis to be up to 100% based on Gd-BOPTA enhanced MRI with liver-specific contrast phase, while confident differential diagnosis was not possible in 70% on the basic of dynamic phase imaging alone [38].

Our study is not without some limitations. Even though for the primary tumor a histopathological correlation was available, due to ethical reasons a histopathological sampling of each detected lesion was not applicable. To overcome this limitation, a well-established modified reference standard was applied [39,40] comprising all available data based on clinical follow-up, imaging and histopathology.

In conclusion our results demonstrate a further increase in diagnostic accuracy for depiction and characterization of liver lesions based on the application of a liver-specific contrast phase in ^{18}F-FDG PET/MR imaging, in addition to standard dynamic contrast-enhanced imaging and DWI. Thus, the application of an enhanced liver imaging protocol in ^{18}F-FDG PET/MR imaging, including the liver specific phase, may improve therapeutic stratification and patient management.

Acknowledgments

This research was supported in part by a sponsored research agreement with Bracco, Milano, Italy. The funders had no role in study design, data collection and analysis, decision to publish, or preparation of the manuscript. This does not alter our adherence to PLOS ONE policies on sharing data and materials. The authors have declared that no competing interests exist.

Author Contributions

Conceptualization: Julian Kirchner, Johannes Grüneisen, Karsten Beiderwellen, Thomas C. Lauenstein, Lale Umutlu.

Data curation: Julian Kirchner, Lino M. Sawicki, Cornelius Deuschl, Johannes Grüneisen.

Formal analysis: Julian Kirchner, Lino M. Sawicki, Cornelius Deuschl.

Funding acquisition: Karsten Beiderwellen, Thomas C. Lauenstein, Michael Forsting, Lale Umutlu.

Investigation: Julian Kirchner, Cornelius Deuschl.

Methodology: Julian Kirchner, Cornelius Deuschl, Johannes Grüneisen.

Project administration: Karsten Beiderwellen, Thomas C. Lauenstein, Ken Herrmann, Philipp Heusch.

Resources: Ken Herrmann, Michael Forsting, Philipp Heusch, Lale Umutlu.

Supervision: Julian Kirchner, Ken Herrmann, Michael Forsting, Philipp Heusch, Lale Umutlu.

Validation: Julian Kirchner, Lino M. Sawicki, Cornelius Deuschl, Johannes Grüneisen, Lale Umutlu.

Visualization: Julian Kirchner, Lale Umutlu.

Writing – original draft: Julian Kirchner, Lale Umutlu.

Writing – review & editing: Julian Kirchner, Lino M. Sawicki, Cornelius Deuschl, Johannes Grüneisen, Karsten Beiderwellen, Thomas C. Lauenstein, Ken Herrmann, Michael Forsting, Philipp Heusch, Lale Umutlu.

References

1. Weiss L, Grundmann E, Torhorst J, Hartveit F, Moberg I, Eder M, et al. (1986) Haematogenous metastatic patterns in colonic carcinoma: an analysis of 1541 necropsies. J Pathol 150: 195–203. https://doi.org/10.1002/path.1711500308 PMID: 3806280
2. Imam K, Bluemke DA (2000) MR imaging in the evaluation of hepatic metastases. Magn Reson Imaging Clin N Am 8: 741–756. PMID: 11149677
3. Riemsma RP, Bala MM, Wolff R, Kleijnen J (2013) Transarterial (chemo)embolisation versus no intervention or placebo intervention for liver metastases. Cochrane Database Syst Rev: CD009498. https://doi.org/10.1002/14651858.CD009498.pub3 PMID: 23633373
4. Ahmed F, Perz JF, Kwong S, Jamison PM, Friedman C, Bell BP (2008) National trends and disparities in the incidence of hepatocellular carcinoma, 1998–2003. Prev Chronic Dis 5: A74. PMID: 18558024
5. Forner A, Llovet JM, Bruix J Hepatocellular carcinoma. The Lancet 379: 1245–1255.
6. van Aalten SM, de Man RA, Ijzermans JNM, Terkivatan T (2012) Systematic review of haemorrhage and rupture of hepatocellular adenomas. British Journal of Surgery 99: 911–916. https://doi.org/10.1002/bjs.8762 PMID: 22619025
7. Grazioli L, Olivetti L, Mazza G, Bondioni MP (2013) MR Imaging of Hepatocellular Adenomas and Differential Diagnosis Dilemma. International Journal of Hepatology 2013: 20.
8. Dokmak S, Paradis V, Vilgrain V, Sauvanet A, Farges O, Valla D, et al. (2009) A Single-Center Surgical Experience of 122 Patients With Single and Multiple Hepatocellular Adenomas. Gastroenterology 137: 1698–1705. https://doi.org/10.1053/j.gastro.2009.07.061 PMID: 19664629
9. Antoch G, Vogt FM, Freudenberg LS, Nazaradeh F, Goehde SC, Barkhausen J, et al. (2003) Whole-body dual-modality PET/CT and whole-body MRI for tumor staging in oncology. JAMA 290: 3199–3206. https://doi.org/10.1001/jama.290.24.3199 PMID: 14693872
10. Niekel MC, Bipat S, Stoker J (2010) Diagnostic imaging of colorectal liver metastases with CT, MR imaging, FDG PET, and/or FDG PET/CT: a meta-analysis of prospective studies including patients who have not previously undergone treatment. Radiology 257: 674–684. https://doi.org/10.1148/radiol.10100729 PMID: 20829538
11. van Kessel CS, Buckens CF, van den Bosch MA, van Leeuwen MS, van Hillegersberg R, Verkooijen HM (2012) Preoperative imaging of colorectal liver metastases after neoadjuvant chemotherapy: a meta-analysis. Ann Surg Oncol 19: 2805–2813. https://doi.org/10.1245/s10434-012-2300-z PMID: 22396005

12. Khalil HI, Patterson SA, Panicek DM (2005) Hepatic lesions deemed too small to characterize at CT: prevalence and importance in women with breast cancer. Radiology 235: 872–878. https://doi.org/10.1148/radiol.2353041099 PMID: 15833992

13. Schwartz LH, Gandras EJ, Colangelo SM, Ercolani MC, Panicek DM (1999) Prevalence and importance of small hepatic lesions found at CT in patients with cancer. Radiology 210: 71–74. https://doi.org/10.1148/radiology.210.1.r99ja0371 PMID: 9885589

14. Heusch P, Antoch G (2015) Morphologic and Functional Imaging of Non-Colorectal Liver Metastases. Viszeralmedizin 31: 387–392. https://doi.org/10.1159/000441857 PMID: 26889141

15. Namasivayam S, Martin DR, Saini S (2007) Imaging of liver metastases: MRI. Cancer Imaging 7: 2–9. https://doi.org/10.1102/1470-7330.2007.0002 PMID: 17293303

16. Neri E, Bali MA, Ba-Ssalamah A, Boraschi P, Brancatelli G, Alves FC, et al. (2016) ESGAR consensus statement on liver MR imaging and clinical use of liver-specific contrast agents. European Radiology 26: 921–931. https://doi.org/10.1007/s00330-015-3900-3 PMID: 26194455

17. Drzezga A, Souvatzoglou M, Eiber M, Beer AJ, Fürst S, Martinez-Möller A, et al. (2012) First Clinical Experience with Integrated Whole-Body PET/MR: Comparison to PET/CT in Patients with Oncologic Diagnoses. Journal of Nuclear Medicine 53: 845–855. https://doi.org/10.2967/jnumed.111.098608 PMID: 22534830

18. Heusch P, Buchbender C, Beiderwellen K, Nensa F, Hartung-Knemeyer V, Lauenstein TC, et al. (2013) Standardized uptake values for [(1)(8)F] FDG in normal organ tissues: comparison of whole-body PET/CT and PET/MRI. Eur J Radiol 82: 870–876. https://doi.org/10.1016/j.ejrad.2013.01.008 PMID: 23394765

19. Grueneisen J, Beiderwellen K, Heusch P, Gratz M, Schulze-Hagen A, Heubner M, et al. (2014) Simultaneous positron emission tomography/magnetic resonance imaging for whole-body staging in patients with recurrent gynecological malignancies of the pelvis: a comparison to whole-body magnetic resonance imaging alone. Invest Radiol 49: 808–815. https://doi.org/10.1097/RLI.0000000000000086 PMID: 25010207

20. Buchbender C, Heusner TA, Lauenstein TC, Bockisch A, Antoch G (2012) Oncologic PET/MRI, part 2: bone tumors, soft-tissue tumors, melanoma, and lymphoma. J Nucl Med 53: 1244–1252. https://doi.org/10.2967/jnumed.112.109306 PMID: 22782313

21. Buchbender C, Heusner TA, Lauenstein TC, Bockisch A, Antoch G (2012) Oncologic PET/MRI, part 1: tumors of the brain, head and neck, chest, abdomen, and pelvis. J Nucl Med 53: 928–938. https://doi.org/10.2967/jnumed.112.105338 PMID: 22582048

22. Beiderwellen K, Gomez B, Buchbender C, Hartung V, Poeppel TD, Nensa F, et al. (2013) Depiction and characterization of liver lesions in whole body [(1)(8)F]-FDG PET/MRI. Eur J Radiol 82: e669–675. https://doi.org/10.1016/j.ejrad.2013.07.027 PMID: 24011443

23. Lee DH, Lee JM, Hur BY, Joo I, Yi NJ, Suh KS, et al. (2016) Colorectal Cancer Liver Metastases: Diagnostic Performance and Prognostic Value of PET/MR Imaging. Radiology 280: 782–792. https://doi.org/10.1148/radiol.2016151975 PMID: 27092659

24. Quick HH (2014) Integrated PET/MR. J Magn Reson Imaging 39: 243–258. https://doi.org/10.1002/jmri.24523 PMID: 24338921

25. Kirchin MA, Pirovano GP, Spinazzi A (1998) Gadobenate dimeglumine (Gd-BOPTA). An overview. Invest Radiol 33: 798–809. PMID: 9818314

26. Caudana R, Morana G, Pirovano GP, Nicoli N, Portuese A, Spinazzi A, et al. (1996) Focal malignant hepatic lesions: MR imaging enhanced with gadolinium benzyloxypropionictetra-acetate (BOPTA)—preliminary results of phase II clinical application. Radiology 199: 513–520. https://doi.org/10.1148/radiology.199.2.8668804 PMID: 8668804

27. Spinazzi A, Lorusso V, Pirovano G, Kirchin M (1999) Safety, tolerance, biodistribution, and MR imaging enhancement of the liver with gadobenate dimeglumine: results of clinical pharmacologic and pilot imaging studies in nonpatient and patient volunteers. Acad Radiol 6: 282–291. PMID: 10228617

28. Ward J (2006) New MR techniques for the detection of liver metastases. Cancer Imaging 6: 33–42. https://doi.org/10.1102/1470-7330.2006.0007 PMID: 16766267

29. Thomeer MG, Broker M, Verheij J, Doukas M, Terkivatan T, Bijdevaate D, et al. (2016) Hepatocellular adenoma: when and how to treat? Update of current evidence. Therapeutic Advances in Gastroenterology 9: 898–912. https://doi.org/10.1177/1756283X16663882 PMID: 27803743

30. Silva AC, Evans JM, McCullough AE, Jatoi MA, Vargas HE, Hara AK (2009) MR imaging of hypervascular liver masses: a review of current techniques. Radiographics 29: 385–402. https://doi.org/10.1148/rg.292085123 PMID: 19325055

31. Beiderwellen K, Geraldo L, Ruhlmann V, Heusch P, Gomez B, Nensa F, et al. (2015) Accuracy of [18F] FDG PET/MRI for the Detection of Liver Metastases. PLoS One 10: e0137285. https://doi.org/10.1371/journal.pone.0137285 PMID: 26335246

32. Antoch G, Stattaus J, Nemat AT, Marnitz S, Beyer T, Kuehl H, et al. (2003) Non-small cell lung cancer: dual-modality PET/CT in preoperative staging. Radiology 229: 526–533. https://doi.org/10.1148/radiol.2292021598 PMID: 14512512

33. Lee KH, Lee JM, Park JH, Kim JH, Park HS, Yu MH, et al. (2013) MR imaging in patients with suspected liver metastases: value of liver-specific contrast agent gadoxetic acid. Korean J Radiol 14: 894–904. https://doi.org/10.3348/kjr.2013.14.6.894 PMID: 24265564

34. Kele PG, van der Jagt EJ (2010) Diffusion weighted imaging in the liver. World Journal of Gastroenterology: WJG 16: 1567–1576. https://doi.org/10.3748/wjg.v16.i13.1567 PMID: 20355235

35. Holzapfel K, Eiber MJ, Fingerle AA, Bruegel M, Rummeny EJ, Gaa J (2012) Detection, classification, and characterization of focal liver lesions: Value of diffusion-weighted MR imaging, gadoxetic acid-enhanced MR imaging and the combination of both methods. Abdom Imaging 37: 74–82. https://doi.org/10.1007/s00261-011-9758-1 PMID: 21597893

36. Bruegel M, Holzapfel K, Gaa J, Woertler K, Waldt S, Kiefer B, et al. (2008) Characterization of focal liver lesions by ADC measurements using a respiratory triggered diffusion-weighted single-shot echo-planar MR imaging technique. European Radiology 18: 477–485. https://doi.org/10.1007/s00330-007-0785-9 PMID: 17960390

37. Donati OF, Hany TF, Reiner CS, von Schulthess GK, Marincek B, Seifert B, et al. (2010) Value of retrospective fusion of PET and MR images in detection of hepatic metastases: comparison with 18F-FDG PET/CT and Gd-EOB-DTPA-enhanced MRI. J Nucl Med 51: 692–699. https://doi.org/10.2967/jnumed.109.068510 PMID: 20395324

38. Grazioli L, Morana G, Kirchin MA, Schneider G (2005) Accurate differentiation of focal nodular hyperplasia from hepatic adenoma at gadobenate dimeglumine-enhanced MR imaging: prospective study. Radiology 236: 166–177. https://doi.org/10.1148/radiol.2361040338 PMID: 15955857

39. Grueneisen J, Sawicki LM, Schaarschmidt BM, Suntharalingam S, von der Ropp S, Wetter A, et al. (2016) Evaluation of a Fast Protocol for Staging Lymphoma Patients with Integrated PET/MRI. PLoS One 11: e0157880. https://doi.org/10.1371/journal.pone.0157880 PMID: 27327617

40. Sawicki LM, Grueneisen J, Schaarschmidt BM, Buchbender C, Nagarajah J, Umutlu L, et al. (2016) Evaluation of (1)(8)F-FDG PET/MRI, (1)(8)F-FDG PET/CT, MRI, and CT in whole-body staging of recurrent breast cancer. Eur J Radiol 85: 459–465. https://doi.org/10.1016/j.ejrad.2015.12.010 PMID: 26781152